ELSEVIER

Journal of Alloys and Compounds 217 (1995) 185–192

Journal of ALLOYS AND COMPOUNDS

The effect of tin on the degradation of $LaNi_{5-y}Sn_y$ metal hydrides during thermal cycling

R.C. Bowman, Jr. [a], C.H. Luo [b], C.C. Ahn [b], C.K. Witham [b], B. Fultz [b]

[a] *Aerojet Electronic Systems, PO Box 296, Azusa, CA 91702, USA*

[b] *Division of Engineering and Applied Science, California Institute of Technology, Pasadena, CA 91125, USA*

Received 24 June 1994

Abstract

Three $LaNi_{5-y}Sn_y$ alloys with $y=0.0$, 0.1 and 0.2 have been subjected to hundreds of hydrogen absorption–desorption reactions during thermal cycling from room temperature to over 500 K. Both $LaNi_5H_x$ and $LaNi_{4.9}Sn_{0.1}H_x$ were cycled until their reversible hydrogen storage capacities had decreased by about 60%. X-ray diffractometry and transmission electron microscopy showed that the resulting degraded hydrides had partially disproportionated into nanocrystalline f.c.c. LaH_x and Ni metal. The substitution of only a small amount of tin suppressed the rate of degradation by more than a factor of 3 for $y=0.1$, and a factor of 20 for $y=0.2$. For all three alloys there was a reasonably consistent correlation between the degree of disproportionation and the degradation in reversible hydrogen capacity. The present study verifies that partial Sn substitution for Ni in $LaNi_5$ produces alloys that are very resistant to intrinsic disproportionation.

Keywords: Tin; Thermal cycling; Metal hydrides

1. Introduction

The exceptional reversible hydrogen absorption properties of $LaNi_5$ and related alloys have made them attractive candidates for numerous energy storage and conversion applications [1]. Many potential applications require the alloys to undergo ten of thousands of hydrogen absorption–desorption reactions during cooling and heating cycles. Cohen and coworkers [2–6] first described the degradation in the reversible hydrogen storage capacities Δx of $La_{0.9}Eu_{0.1}Ni_{4.6}Mn_{0.4}H_x$ and $LaNi_5H_x$ that occurred during thermal cycling. From Mössbauer spectroscopy and magnetization studies, the reduced hydrogen storage was attributed to the intrinsic disproportionation reaction

$$LaNi_5H_x \longrightarrow LaH_2 + 5Ni + H_2 \quad (1)$$

However, Cohen and coworkers were unable to identify the decomposition products LaH_2 or Ni metal using X-ray diffraction.

Other researchers subjected $LaNi_5$ and several of its alloys to either thermal cycling or thermal anneals under hydrogen pressure, and similar decreases in Δx were found [7–17]. The extent and nature of the degradation observed during these studies was strongly dependent upon experimental factors that include (1) purity of hydrogen gas and quality of vacuum, (2) temperature range (especially the upper limit), (3) cycle repetition times and heating or cooling rates, (4) the nominal pressures and (5) perhaps other unspecified variables related to the preparation and handling of the alloys. Consequently, it has been difficult to make reliable predictions of the degradation of $LaNi_5$ alloys under general conditions, and much remains unknown about the mechanisms responsible for degradation. While it is known that impurities from contamination sources promote the formation of segregated phases of oxides and Ni clusters on the surfaces of the alloy particles [18], deterioration of the storage capacity occurs even when these impurities are controlled. The metastable ternary $LaNi_5$ hydride phase is also susceptible to various disordering processes that create microstrains and lattice defects upon hydriding [19,20]. Some researchers [7–9] attributed the cycling-induced changes in the $LaNi_5H_x$ isotherms primarily to extensive lattice disorder and hydrogen trapping at defects rather than the disproportionation reaction given by Eq. (1). Nevertheless, several other studies [13–16] have clearly shown the presence of intense Ni metal peaks in the X-ray diffraction patterns of heavily degraded $LaNi_5H_x$. The large concentrations of f.c.c. Ni metal clearly support the assertion that disproportionation does occur,

SSDI 0925-8388(94)01337-3

at least under some experimental conditions. The formation of the non-stoichiometric LaH_x phase with x between about 1.8 and 3 has been harder to prove. The quality of the X-ray diffraction patterns from the cycled material is impaired by the combination of small domains, distributions of large lattice strains, and peak overlaps from the multiple phases. Unambiguous identification of the decomposition products is therefore difficult. In a diffraction pattern obtained from a $LaNi_5H_x$ sample that had been cycled 3150 times between 303 and 473 K to produce an 87% degradation in hydrogen storage capacity, Ahn and Lee [13] recently assigned some weak diffraction peaks to precipitated LaH_2 and $LaNiH_{3.6}$ phases.

While alloying is widely known to alter the absorption and desorption plateau pressures of the $LaNi_5$ hydrides [1,14,16,21,22], most elements that are substituted for either La or Ni do not increase the stability of the alloy during thermal cycling. The most notable exceptions are partial Al and Sn substitutions for Ni. Although both elements reduce the degradation [7,11,14], the results of Lambert et al. [14] indicate that tin at $y \approx 0.2$ is especially effective. The objectives of the present study were to examine the role of Sn substitution on the cycling behavior of the $LaNi_{5-y}Sn_y$ hydrides under more severe conditions than had been used by Lambert et al., and to correlate these changes in hydrogen storage capacity to the microstructural changes in the alloy.

2. Experimental details

Three $LaNi_{5-y}Sn_y$ alloys with $y = 0.0$, 0.1 and 0.2 were obtained from the Ames Laboratory of Iowa State University. Arc-melted ingots of each alloy had been prepared using appropriate amounts of high purity (e.g. greater than 99.95 at.%) metals. Optical metallography and X-ray diffractometry showed that all three $LaNi_{5-y}Sn_y$ alloys were single phase after the ingots had been vacuum annealed for several days at 1170 K ($y = 0.1$) or 1220 K ($y = 0.0$ and 0.2). Pieces of the ingots were ground into -100 mesh powder for loading into an electropolished type 316L stainless steel reaction vessel. The initial activation of the powder consisted of several evacuation and hydrogen absorption cycles using a high-vacuum-compatible gas-handling system based upon a turbomolecular vacuum pump station and with MKS Instruments model 315 baratron high precision capacitance manometers. After activation, the reactor was opened in a glove-box with an argon atmosphere containing oxygen and water levels below 1.0 ppm and 0.1 ppm respectively. Portions of the activated $LaNi_{5-y}Sn_y$ powder were retained for characterization by X-ray diffraction, surface area measurements by the Brunauer–Emmett–Teller method, and scanning electron microscopy and transmission electron microscopy (TEM) examinations. After the mass of the nominal 5 g of activated alloy powder was accurately determined, each sample was returned to the reactor vessel for isotherm measurements and thermal cycling.

A schematic drawing of the system used for the thermal cycling experiments is shown in Fig. 1. The gas manifold and calibrated volumes were assembled with electropolished type 316L stainless steel and metal gasket face seal cajon VCR fittings. A Tribodyn oil-free vacuum pump with a base pressure below 10^{-4} Torr was attached to the manifold. A Setra model 212FT pressure transducer was used to monitor the pressure to over 35 atm. Research grade (99.995% purity) hydrogen was supplied to the system through a clean stainless steel pressure regulator. For isotherm measurements between 298 and 363 K, the reaction vessel was submerged in a thermally regulated water bath. Thermal cycling between temperatures above 500 K to room temperature (i.e. 293–295 K) was performed with a resistively heated copper tube furnace that enclosed the reactor vessel. Cooling was provided by a fan that blew air inside the copper sleeve and over the reactor. Type K (i.e. chromel–alumel) thermocouples provided temperature data to the Macintosh SE computer with a Data Translation analog-to-digital converter board. Pressure data from the Setra transducer were also acquired through this board. Digital outputs from this board controlled the heater and fan. A temperature cycle consisted of heating for 40 min to the nominal 500 K upper temperature followed by fan cooling for 40 min, which returned the temperature to about 295 K. The thermocouple in the center of the reactor vessel showed that about 90% of the temperature change in the heating and cooling transitions occurred within 5–10 min. Table 1 presents the hydrogen pressure P_{low} over the $LaNi_{5-y}Sn_yH_x$ just before starting the thermal cycling, the nominal high temperature limit T_{high}, the pressure P_{high} at T_{high}, and the reversible change Δx in hydrogen content obtained from the

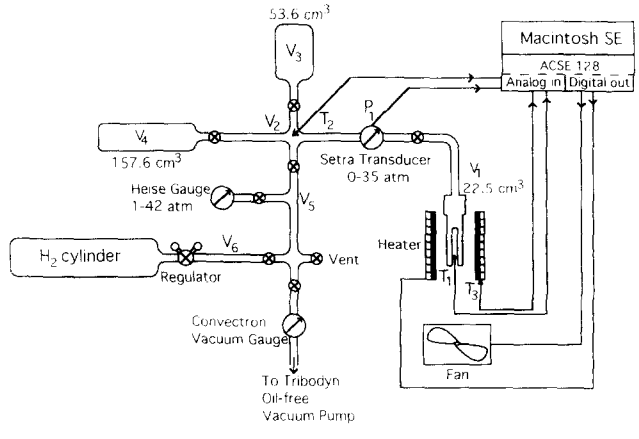

Fig. 1. Schematic drawing of the experimental system used for the thermal cycling and isotherm measurements.

Table 1
Pressures, temperatures and reversible hydrogen contents Δx of the first and last thermal cycles for the three $LaNi_{5-y}Sn_yH_x$ samples

Alloy composition	Cycle number	P_{low} (atm)	T_{low} (K)	P_{high} (atm)	T_{high} (K)	Δx
$LaNi_{5.0}$	1	15.6	297	29.3	508	6.96
	520	16.4	296	24.6	504	3.05
$LaNi_{4.9}Sn_{0.1}$	1	12.9	297	25.5	502	6.64
	1453	16.0	295	21.4	542	1.96
$LaNi_{4.8}Sn_{0.2}$	1	16.9	294	30.4	511	6.29
	1330	17.4	297	29.7	509	5.65

measured pressures in the first thermal absorption–desorption cycle.

The X-ray diffraction measurements were performed using an Inel CSP-120 Debye–Scherrer powder diffractometer system with a sealed tube source of Co Kα radiation and an incident beam monochromater. The position-sensitive detector had a window that subtended 127° in 2θ angle with a resolution of 0.04°.

The microstructures of activated and cycled $LaNi_{5-y}Sn_yH_x$ powders were studied with a Philips EM430 transmission electron microscope operating at 300 keV. This instrument included an EDAX model 9900 energy-dispersive X-ray analyser that was used to determine the relative ratios of the metals in various regions of interest. The TEM specimens were prepared by grinding the friable $LaNi_{5-y}Sn_yH_x$ powders as suspensions in the volatile and inert fluorocarbon liquid Fluorinert FC-43 (3M Industrial Chemical Products, St. Paul, MN). Since the powders had been placed into this liquid while they were inside the argon-atmosphere glove-box, air exposure of the particles was minimized before the finely ground samples were inserted into the TEM vacuum stage.

3. Results

3.1. Hydrogen storage capacity studies

Each of the $LaNi_{5-y}Sn_y$ alloys was found to react readily with hydrogen both during the first absorption of the activation procedure, and in the first cycle after the activated powders were reloaded for the thermal cycling experiments. The hydrogen absorption and desorption isotherms obtained before starting the thermal cycling treatments gave pressures and storage capacities that were consistent with previous studies [14,21,22] of the $LaNi_{5-y}Sn_y$–H_2 system. The Sn substitution caused a reduction in the plateau pressures, decreased hysteresis factors and a slightly diminished hydrogen storage capacity.

After pressure–composition isotherms had been measured to establish the initial widths and pressures of the absorption and desorption plateaux, thermal cycling was initiated without disturbing the reactor vessel or the gas manifold. Each $LaNi_{5-y}Sn_y$ alloy was cycled between room temperature and the nominal upper temperature listed in Table 1. Representative data on the pressures and temperatures obtained during thermal cycles 10–14, 515–519 and 1325–1329 for all three $LaNi_{5-y}Sn_y$ alloys are compared in Fig. 2. The pressure data show directly the degradation in reversible hydrogen storage capacity. Figure 2(a) for $LaNi_5H_x$ shows that by the 515th cycle the maximum pressure at high temperatures is decreased substantially (i.e. the desorbed condition for the hydride is incomplete, as hydrogen is being held in the solid phase). Meanwhile, the minimum pressures at room temperature increased noticeably (i.e. the hydrogen content in the fully absorbed condition is reduced). Figure 2(b) shows that the $LaNi_{4.9}Sn_{0.1}$ hydride phase underwent much less degradation after 500 cycles between 295 and 540 K. Degradation to the reversible storage capacity of $LaNi_5H_x$ after about 500 cycles occurred in $LaNi_{4.9}Sn_{0.1}H_x$ only after about 1300 cycles. Furthermore, Fig. 2(c) shows that only about 10% degradation had occurred in $LaNi_{4.8}Sn_{0.2}H_x$ after more than 1325 cycles. The data in Fig. 2 also reveal that the thermal cycling did not alter significantly the kinetics for hydrogen absorption or desorption for any of the materials, even when the storage capacities were reduced up to 60%.

The impact of Sn substitution on the reversible hydrogen capacity Δx for all thermal cycles is shown in Fig. 3. $LaNi_5H_x$ is seen to undergo a steady decrease in Δx from 7.0 to 3.0 during 520 cycles to give a 57% reduction in reversible capacity. However, the change in Δx is much slower for $LaNi_{4.9}Sn_{0.1}H_x$, so that an

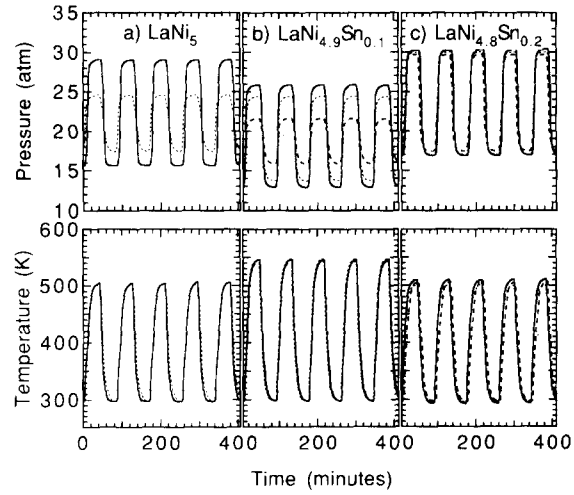

Fig. 2. Comparisons of the pressure and temperature changes observed during representative thermal cycles for (a) $LaNi_5H_x$, (b) $LaNi_{4.9}Sn_{0.1}H_x$ and (c) $LaNi_{4.8}Sn_{0.2}H_x$. The results are for cycles 10–14 (——), 515–519 (-----) and 1325–1329 (– – –).

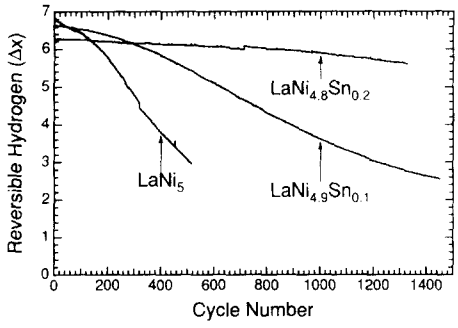

Fig. 3. Hydrogen concentration changes Δx for $LaNi_{5-y}Sn_yH_x$ obtained from the maximum and minimum pressures for each cycle.

equivalent decrease in Δx does not occur until after more than 1350 thermal cycles. While the initial Δx for $LaNi_{4.8}Sn_{0.2}H_x$ was only 6.3 (i.e. about 10% smaller than for $LaNi_5H_x$), it decreased by only 10% during 1330 thermal cycles. The results in Fig. 3 substantiate and extend the previous observation by Lambert et al. [14] that Sn is very effective in suppressing deterioration of the reversible hydrogen storage capacity during cycling to temperatures exceeding 500 K. The values of Δx at the completion of our cycling measurements are listed in Table 1.

Absorption–desorption isotherms obtained before and after thermal cycling of the three $LaNi_{5-y}Sn_yH_x$ samples are presented in Fig. 4. The degradation in Δx, shown in Fig. 3, is clearly accompanied by a severe shortening in the plateau widths and increases in their slopes, which is similar to the behavior found by others [7,10,11–15]. The average pressures near the middle of the plateaux, however, were not changed significantly. Owing to difficulties in correcting properly for all the changes in hydrogen volumes between the thermal cycling and isotherm measurements, the absolute hydrogen contents for the beginnings and ends of the plateaux are imprecise. However, the relative changes in Δx should be reliable. In particular, the nominal 60% decrease in Δx for $LaNi_5H_x$ and $LaNi_{4.9}Sn_{0.1}H_x$ after cycling corresponds well to the residual plateau widths in Fig. 4 that were measured after cycling. The changes in Δx and plateau width are both about 10% for $LaNi_{4.8}Sn_{0.2}H_x$, whose isotherms in Fig. 4(c) showed virtually no changes in the plateau absorption and desorption pressures after more than 1330 cycles.

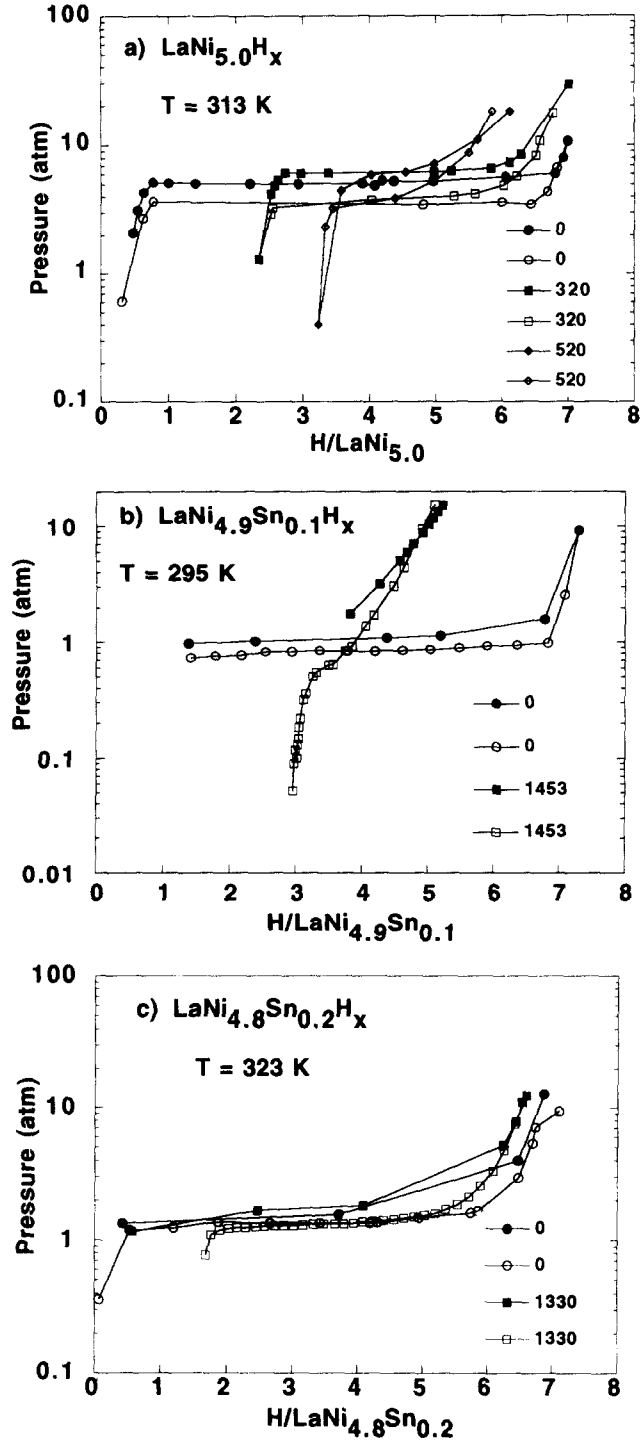

Fig. 4. The absorption (●, ■, ◆) and desorption (○, □, ◇) isotherms for (a) $LaNi_5H_x$ measured at 313 K before thermal cycling and after 320 and 520 cycles, (b) for $LaNi_{4.9}Sn_{0.1}H_x$ obtained at 298 K before cycling and after 1453 cycles and (c) for $LaNi_{4.8}Sn_{0.2}H_x$ obtained at 323 K before cycling and after 1330 cycles.

3.2. Microstructural characterization studies

X-ray diffraction patterns measured from the $LaNi_{5-y}Sn_yH_x$ samples after activation and after thermal cycling are presented in Fig. 5. All diffraction peaks from the activated $LaNi_{5-y}Sn_y$ powders were indexed to the same hexagonal Haucke phase structures as the virgin alloys. The lattice parameters obtained after activation were essentially identical with the values previously determined [23] for the starting alloys. The most significant difference caused by activation was some broadening of the diffraction peaks consistent with the creation of lattice defects and microstrains [19,20]. Thermally cycled $LaNi_{5.0}$ and $LaNi_{4.9}Sn_{0.1}$, both

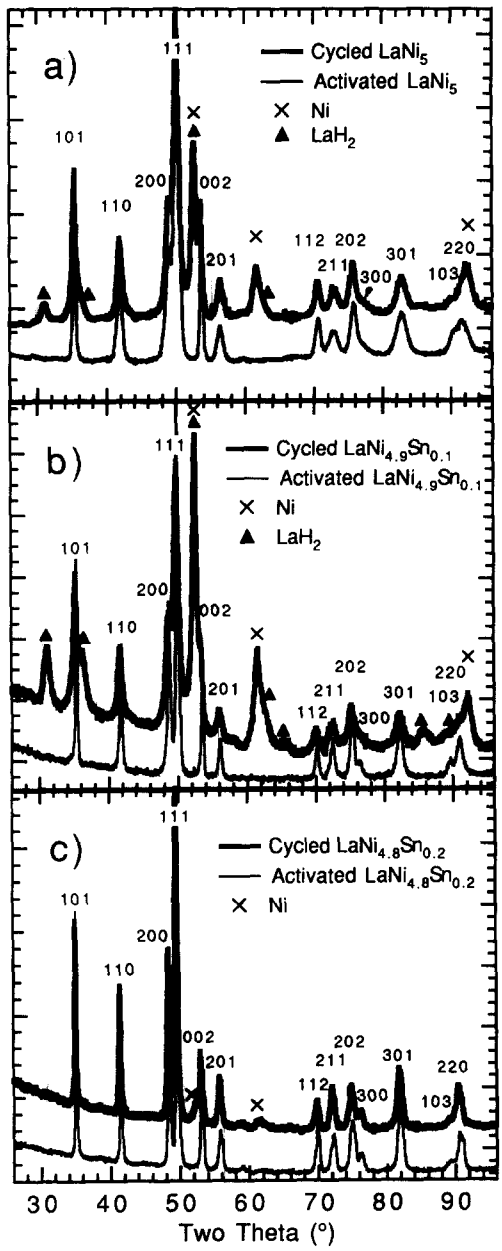

Fig. 5. X-ray diffraction patterns for (a) $LaNi_5$, (b) $LaNi_{4.9}Sn_{0.1}$ and (c) $LaNi_{4.8}Sn_{0.2}$ obtained after activation and after thermal cycling and isotherm measurements.

of which had undergone about 60% degradation in reversible hydrogen storage capacity, had several additional peaks of moderate to strong intensity in their diffraction patterns as indicated in Figs. 5(a) and 5(b). These new peaks are indexed to the expected peaks of the f.c.c. phases LaH_x and Ni, as originally proposed by Cohen and coworkers [2–4]. The diffraction patterns from these heavily degraded samples did not contain any peaks that could be associated with the $LaNiH_x$ phases recently reported by Ahn and Lee [13]. While the peaks from the hexagonal phases also remained prominent in the X-ray diffraction patterns from these cycled samples, these peaks were further broadened compared with the activated material. In contrast, the X-ray diffraction pattern in Fig. 5(c) for $LaNi_{4.8}Sn_{0.2}H_x$ after 1330 thermal cycles had much weaker Ni diffraction peaks, and no detectable peaks from the LaH_x phase. Furthermore, little additional broadening of the diffraction peaks from the hexagonal Haucke phase is seen in Fig. 5(c) after cycling. These results are fully consistent with an enhanced stability of $LaNi_{4.8}Sn_{0.2}H_x$ against the disproportionation reaction of Eq. (1).

Analytical TEM with energy-dispersive X-ray analysis (EDXA) was used to determine spatial variations in the La-to-Ni concentration ratio. This work was performed in microbeam mode, where a 20 nm probe was moved to various parts of the powder particles and an energy-dispersive X-ray spectrum was obtained. These energy-dispersive X-ray measurements must be regarded as qualitative, however, because the spatial scale of the disproportionation reaction is comparable with or smaller than our probe size and specimen thickness. Therefore no effort was made to calibrate these concentration measurements, but local variations in the intensity ratios of La L edge X-rays to Ni K edge X-rays were examined instead. The La-to-Ni concentration ratios were found to differ by less than 5% between several locations in the activated powders, and the energy-dispersive X-ray spectra from the three different alloys in their activated state were very similar. On the contrary, in the cycled degraded hydrides of $LaNi_5$ and $LaNi_{4.9}Sn_{0.1}$, a few spectra were obtained from regions near edges of particles where the La L edge X-rays were less than half the intensity as from other regions, indicating that these regions were Ni rich. Although searches were made for regions with reduced Ni concentration (i.e. La-rich regions), none was found. These results could indicate that the La-rich regions are especially small; so they could not be pinpointed using our experimental technique. Much smaller variations in La-to-Ni ratios were observed for the cycled $LaNi_{4.8}Sn_{0.2}H_x$ material.

Extensive TEM studies were performed on the $LaNi_{4.8}Sn_{0.2}H_x$ samples after activation and after the thermal cycling. The activated alloys contained mostly large homogeneous domains, although the oxidized edges of the powder particles often had fine-grained structures [18]. Similar large-domain microstructures were consistently observed from numerous $LaNi_{4.8}Sn_{0.2}H_x$ particles that were examined by TEM after 1330 cycles, consistent with the X-ray diffraction evidence that no significant phase separation or microsegregation occurred during thermal cycling.

On the contrary, our TEM studies showed that the microstructures of the alloys $LaNi_5$ and $LaNi_{4.9}Sn_{0.1}$ had undergone significant changes after 530 cycles and 1450 cycles respectively. Since very similar TEM images were obtained from both degraded hydrides, only the results from $LaNi_{4.9}Sn_{0.1}H_x$ after the 1453 thermal cycles

and isotherm measurements are presented in this paper. Representative bright-field (BF) and dark-field (DF) images, and a typical selected-area diffraction (SAD) pattern are shown in Fig. 6. The DF image in Fig. 6(b), together with the inset microbeam diffraction pattern, show unambiguously the precipitation of Ni metal. The DF image was formed with the SAD aperture covering the Ni(111) diffraction ring, but with this method it was not possible to suppress all diffractions from the hexagonal Haucke AB_5 phase. Nevertheless, such DF images showed sharply defined regions of 10 nm and larger dimensions. These regions had a distinctly different appearance from other regions with more mottled image contrast. One such especially large particle, oriented for strong diffraction, can be seen at the upper right of Fig. 6(b). We obtained a microbeam diffraction pattern from this individual particle. This pattern, which is inset in Fig. 6(b), indexes consistently to the expected spot spacings and angles for an elemental Ni particle with a (110) zone-axis orientation. The Haucke phase does not have any such diffraction pattern.

TEM offered less direct evidence for the presence of the f.c.c. LaH_2 phase in cycled $LaNi_{4.9}Sn_{0.1}H_x$. The DF image shown in Fig. 6(c) was formed with the (111) and (200) diffractions from f.c.c. LaH_2, which form the innermost rings in SAD patterns such as that presented in the inset. Although these diffractions from f.c.c. LaH_2 occurred at smaller angles than the lowest-order diffractions from the Haucke phase, it is possible that some diffuse background intensity from the more abundant Haucke phase did contribute to the contrast in the DF image in Fig. 6(c). Nevertheless, Fig. 6(c) shows that the regions of f.c.c. LaH_2 are typically quite small, i.e. only a few nanometers in size. These dimensions are not entirely consistent with the presence of sharp diffraction peaks from LaH_2 in the X-ray diffraction pattern shown in Fig. 5(b); the line shape of the X-ray peak is not as severely broadened as would be expected from particles that are as small as in Fig. 6(c). The discrepancy suggests that a broad size distribution exists for the f.c.c. particles in which only the larger LaH_2 particles contribute significantly to the X-ray diffraction pattern. Variations in the detectability of the LaH_2 phases by X-ray diffraction may explain why the LaH_2 and Ni diffraction peaks are not observed in fixed intensity ratios, and why the large range of low pressures occur in the P–x isotherms for cycled samples with $x=0.0$ and $y=0.1$ when so seemingly little f.c.c. LaH_x is detected.

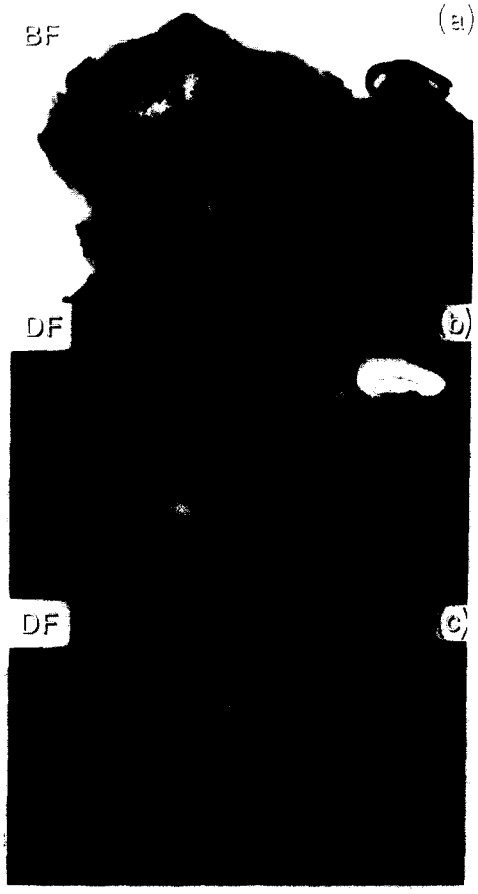

Fig. 6. TEM images for $LaNi_{4.9}Sn_{0.1}H_x$ obtained after 1453 thermal cycles (see text for details).

4. Discussion

The present studies have demonstrated that nanocrystals of both LaH_x and Ni metal are produced when $LaNi_5H_x$ is thermally cycled to temperatures of around 500 K. These phases were identified in two of our three alloys. We expect that the disproportionation reaction in Eq. (1) will occur under most conditions of hydrogen absorption–desorption cycling. The fact that these reaction products were not observed in many previous studies is probably caused by limited growth of LaH_x and Ni clusters to sizes that can be readily detected by X-ray diffraction. The nucleation and growth of the particles of LaH_x and Ni will be strongly dependent on the diffusion rate for the metal atoms within the ternary hydride. We believe that the severe cycling conditions of the present thermal cycling promoted more metal atom diffusion than may have occurred at the lower maximum temperatures (i.e. below 400 K) that were used in some previous work [7,9,10]. It may be that the combination of higher temperatures, longer times and higher hydrogen concentration used in the present work led to more movement of metal atoms and therefore larger and more readily identifiable particles of Ni and LaH_x. We suggest that much of the apparent differences in disproportionation behavior found by past researchers can be explained by the differences in sizes of the reaction products in Eq. (1). The kinetics of nucleation, growth and coarsening of

the reaction products would be quite different under various experimental conditions. At low temperatures, we expect the reaction products are simply too small for convenient detection.

The present cycling experiments also confirm and extend the observations by Lambert et al. [14] that small amounts of Sn substitution (i.e. $y \approx 0.1$–0.2) greatly inhibit the intrinsic disproportionation of $LaNi_{5-y}Sn_y$ during thermal cycling. The effect is quite remarkable in that $LaNi_{4.8}Sn_{0.2}H_x$ is almost immune to degradation under conditions where $LaNi_5H_x$ has suffered a 60% degradation and $LaNi_{4.9}Sn_{0.1}H_x$ has lost about 15% of its reversible capacity. Since the free energy for the disproportionation of $LaNi_5H_x$ is estimated [6,24] to be about -96 kJ mol^{-1} H_2, it seems unreasonable that a mere 4% substitution of Sn for Ni could suppress thermodynamically such a favorable reaction. We believe that Sn atoms must be altering the kinetics for disproportionation by reducing substantially the metal atom mobilities, or perhaps by retarding the nucleation kinetics of the reaction products.

Although the rate of decomposition is decreased significantly for $LaNi_{4.9}Sn_{0.1}H_x$, the same products LaH_x and Ni are formed in both alloys. The correlation between the disproportionation in our three alloys and the loss of reversible hydrogen storage capacity is best demonstrated by comparing the change in Δx (from Table 1) with the intensity of X-ray diffraction peaks from either Ni or LaH_x in Fig. 5. Although this comparison does not yield a linear dependence (since the $LaNi_{4.9}Sn_{0.1}$ alloy showed less deterioration in Δx than would be expected from its abundance of Ni and LaH_x), the qualitative relationship between these parameters is reasonably good. The deterioration in Δx correlates closely with the extent of the disproportionation reaction. The same disproportionation reaction seems to occur in the presence of Sn, but at a slower rate. Further elucidation of the atomistic mechanism by which Sn retards metal atom movements or impedes the nucleation of the reaction products will require more detailed knowledge of the Sn locations within the hexagonal alloy lattice and other chemical information. Nevertheless, Sn has been shown to be more effective in retarding intrinsic degradation over a wider range of conditions than Al substitution [7,11] which previously gave the largest improvement in stability during thermal cycling.

5. Summary

Dilute substitutions of Sn for Ni in $LaNi_5$ were shown to provide dramatic improvements in the stability of the ternary hydride phase during hydrogen absorption and desorption by thermal cycling from room temperature to over 500 K. The degradation in the reversible hydrogen storage capacity Δx was suppressed by a factor of 20 for $LaNi_{4.8}Sn_{0.2}$ in comparison with the degradation of binary $LaNi_5$. This degradation in Δx involved an increase in the low pressure region before the distorted plateau in the P–x isotherm, consistent with the formation of the thermodynamically stable f.c.c. LaH_x phase. The high concentration limits of the plateaux were found to decrease for the degraded alloys and the residual plateaux also had increased slopes. These effects are consistent with the presence of defects and composition inhomogeneities in the cycled Haucke phase.

X-ray diffractometry and TEM showed that a disproportionation reaction, leading to the formation of f.c.c. LaH_x and elemental Ni, accompanied the degradation in Δx. There was reasonable consistency between the amount of these reaction products and the amount of degradation in the three alloys studied, although the reaction products may not have the same detectability in different alloys owing to variations in their size. We suggest it is unlikely that such a small amount of Sn will have a strong effect on the thermodynamic stability of $LaNi_5$ against disproportionation; so the Sn atoms probably affect the kinetics of nucleation or diffusional growth of the reaction products.

Acknowledgments

We thank T.W. Ellis and B.J. Beaudry of the Ames Laboratory, Iowa State University, for preparation of the alloys. D. Labor assisted with the experimental studies that were performed at Aerojet. The support and helpful comments by M. Canon are appreciated. This work was supported by Aerojet Independent Research and Development (IRAD) funds and the National Science Foundation under Grant DMR-9213447.

References

[1] G. Sandrock, S. Suda and L. Schlapback, in L. Schlapbach (ed.), *Hydrogen in Intermetallic Compounds II*, Springer, Berlin, 1992, p. 197.
[2] R.L. Cohen, K.W. West and J.H. Wernick, *J. Less-Common Met., 70* (1980) 229.
[3] R.L. Cohen, K.W. West and J.H. Wernick, *J. Less-Common Met., 73* (1980) 273.
[4] H. Rummel, R.L. Cohen, P. Gütlich and K.W. West, *Appl. Phys. Lett., 40* (1982) 477.
[5] R.L. Cohen, R.C. Sherwood and K.W. West, *Appl. Phys. Lett., 41* (1982) 999.
[6] R.L. Cohen and K.W. West, *J. Less-Common Met., 95* (1983) 17.
[7] P.D. Goodell, *J. Less-Common Met., 99* (1984) 1.
[8] M.J. Benham, D.K. Ross, C. Lartique and A. Percheron-Guegan, *Z. Phys. Chem., NF, 147* (1986) 191.
[9] J.E. Bonnet, P. Dantzer, H. Dexpert, J.M. Esteva and R. Karnatak, *J. Less-Common Met., 130* (1987) 491.

[10] Y. Josephy, E. Bershadsky and M. Ron, *J. Less-Common Met., 172–174* (1991) 997.
[11] J.-M. Park and J.-Y. Lee, *Mater. Res. Bull., 22* (1987) 455.
[12] J.I. Han and J.-Y. Lee, *Int. J. Hydrogen Energy, 13* (1988) 577.
[13] H.-J. Ahn and J.-Y. Lee, *Int. J. Hydrogen Energy, 16* (1991) 93.
[14] S.W. Lambert, D. Chandra, W.N. Cathey, F.E. Lynch and R.C. Bowman, Jr., *J. Alloys Comp., 187* (1992) 113.
[15] D. Chandra, S. Bagchi, S.W. Lambert, W.N. Cathey, F.E. Lynch and R.C. Bowman, Jr., *J. Alloys Comp., 199* (1993) 93.
[16] W. Luo, S. Luo, J.D. Clewley, T.B. Flanagan, R.C. Bowman, Jr. and J.S. Cantrell, *J. Alloys Comp., 202* (1993) 147.
[17] H. Uchida, K. Terao and Y.C. Huang, *Z. Phys. Chem., NF, 164* (1989) 1275.
[18] P. Selvam, B. Viswanathan, C.S. Swamy and V. Srinivasan, *Int. J. Hydrogen Energy, 16* (1991) 23.
[19] E.H. Kisi, C.E. Buckley and E.M. Gray, *J. Alloys Comp., 185* (1992) 369.
[20] G.-H. Kim, C.-H. Chun, S.-G. Lee and J.-Y. Lee, *Scr. Metall. Mater., 29* (1993) 485.
[21] M.H. Mendelsohn, D.M. Gruen and A.E. Dwight, *Mater. Res. Bull., 13* (1978) 1221.
[22] M. Mendelsohn, D. Gruen and A. Dwight, *Inorg. Chem., 18* (1979) 3343.
[23] J.S. Cantrell, T.A. Beiter and R.C. Bowman, Jr., *J. Alloys Comp., 207/208* (1994) 372.
[24] H.Y. Zhu, J. Wu and Q.D. Wang, *J. Alloys Comp., 185* (1992) 1.